Evaluation of cavitation erosion resistance of Al-Si casting alloys: effect of eutectic and intermetallic phases

Marialaura Tocci, Annalisa Pola, Lorenzo Montesano, G. Marina La Vecchia
Department of Mechanical and Industrial Engineering, University of Brescia, Via Branze 38, 25123, Brescia, Italy
m.tocci@unibs.it, http://orcid.org/0000-0002-7515-0615
annalisa.pola@unibs.it, http://orcid.org/0000-0002-0722-6518
lorenzo.montasano@unibs.it, http://orcid.org/0000-0001-5465-6265
marina.lavecchia@unibs.it, http://orcid.org/0000-0001-5919-0396

ABSTRACT. In the present paper, the influence of eutectic and intermetallic phases on cavitation resistance of Al-Si alloys was studied. In fact, Al-Si alloys are commonly used for the production of components, such as cylinders, pistons, pumps, valves and combustion chambers, which in service may incur in cavitation phenomenon. Samples of AlSi3, AlSi9 and AlSi9CuFe were characterized from the microstructural point of view. Hardness measurements were also performed. Subsequently, cavitation tests were carried out according to ASTM G32 standard and the erosion mechanism was examined by scanning electron microscope.
It was found the both eutectic and intermetallic phases enhance cavitation resistance, expressed in terms of mass loss. Particularly, intermetallic particles with complex morphologies provide a positive contribution, exceeding that of other microstructural features, as grain size.
The effect of T6 heat treatment was also evaluated. It was confirmed that the precipitation of fine strengthening particles in the Al matrix successfully hinders the movement of dislocations, resulting in a longer incubation stage and a lower mass loss for heat-treated samples in comparison with as-cast ones. Finally, the relationship between cavitation resistance and material hardness was investigated.

KEYWORDS. Cavitation erosion; Scanning Electron Microscopy; Al-Si alloys; Brinell hardness; Intermetallics.

OPEN ACCESS

Citation: Tocci, M., Pola, A., Montesano, L., La Vecchia, G. M., Evaluation of cavitation erosion resistance of Al-Si casting alloys: effect of eutectic and intermetallic phases, Frattura ed Integrità Strutturale, 43 (2018) 218-230.

Received: 15.11.2017
Accepted: 06.12.2017
Published: 01.01.2018

INTRODUCTION

Cavitation erosion is a mechanical damage that occurs when a component is in contact with a liquid in particular pressure conditions [1] since gas or vapor bubbles can nucleate and subsequently collapse due to pressure fluctuations in the fluid. The energy associated to this bubbles collapse is significant and it can cause remarkable stress on the surface of the metallic component located in the surrounding areas [2]. In fact, these violent collapses produce

liquid micro-jets that are directed toward the surface, leading to its progressive roughening and plastic deformation [3-4]. The repetition of this loading condition can cause material removal and, finally, the failure of the component itself [5]. Typical components that can be exposed to cavitation erosion are hydrofoils, pipelines, hydraulic pumps, and valves [1].
Various studies are available in scientific literature regarding the characterization of cavitation erosion resistance of different alloys, as such as steels [6-7], cast irons [8], titanium and nickel alloys [3, 9-10]. Furthermore, numerous attempts to develop cavitation erosion models based on bulk mechanical properties [11-13] were performed in order to predict the erosion performance of metallic materials. At this regard, some authors report the hardness as an indicator of the erosion resistance. Nevertheless, these models reached limited success in prediction erosion damage, as well as the attempt to correlate cavitation resistance and hardness [14-15].
Damage due to cavitation can occur also on various aluminum automotive components, as such as cylinders and pistons, combustion chambers, etc. [1, 16]. For this reason, over the years, several studies have been performed in order to investigate the cavitation erosion resistance also of aluminum alloys and to correlate it to microstructural and mechanical properties. Concerning the family of wrought alloys, various alloys belonging to the Al-Cu, Al-Mg, Al-Si-Mg or Al-Zn-Mg families were tested in different conditions [14, 17] taking also into account the influence of real erosion environments, as for instance the presence of aggressive fluids or slurries [8, 18]. For casting alloys, in general, it was found that Al alloys resistance is strongly affected by several microstructural properties, as such as grain size, number of interfaces between different phases, presence and morphology of secondary phases [14-15, 19-20]. This is not surprising since various studies report the influence of eutectic [21-22] and intermetallic phase [23-25], as well as the role of grain size [26-27], on other mechanical properties. It should also be mentioned that casting manufacturing produces defects like porosities, non-metallic inclusions, and segregations [28] that could represent preferential site for erosion damage. In order to enhance microstructural and mechanical properties of casting alloys, the effect of Al-Si composites reinforced with particles or fibers of silicon carbide and alumina was also evaluated [29-30].
Furthermore, it is well known that a proper choice of heat treatment parameters can increase several mechanical properties [31-33]. For this reason, the influence of heat treatment on cavitation resistance was investigated and various studies demonstrated the beneficial contribution of age hardening on reducing material damage [14, 19-20].
Considering the erosion mechanism, under continuous exposure to cavitation, it is reported in scientific literature that the initial undulations of the exposed surface gradually develop into craters and material is lost by necking of the rims of the craters, flaking and dislodging of secondary phases [1, 3, 14, 19]. Hence, it appears evident a dependency of cavitation-erosion behavior on the alloy microstructure, not simply related to the heat treatment effect. Nevertheless, a complete characterization of the erosion mechanism of Al casting alloys as a function of eutectic and intermetallic phases is not available in scientific literature. Therefore, in the present study, the cavitation resistance of different Al-Si alloys was evaluated in order to individuate the effect of Si and intermetallic particles on erosion resistance.

MATERIALS AND METHODS

The cavitation erosion resistance of three Al-Si-Mg alloys with different contents of alloying elements was evaluated. In particular, the performance of AlSi3Mg and AlSi9Mg alloys, with 3 and 9 wt. % Si respectively, was studied in order to investigate the effect of Si content, i.e. the eutectic content, on erosion resistance. On the other hand, the addition of Cu and Fe to AlSi9Mg alloy allowed the authors to examine also the influence of intermetallic particles. The mean chemical composition of the tested alloys, measured by an optical emission spectrometer, is shown in Tab. 1.

	Si	Mg	Cu	Fe	Mn	Ti	Al
AlSi3Mg	3.39	0.64	--	0.09	--	0.09	Balance
AlSi9Mg	8.80	0.29	--	0.08	--	0.10	Balance
AlSi9CuFe	8.80	0.30	0.90	0.53	0.3	0.10	Balance

Table 1: Main alloying elements (wt. %) for the studied alloys.

Samples of the alloys were gravity cast in a permanent mould as cylinders, with diameter of 26 mm and height of 60 mm. In all cases, the mould was pre-heated at 180°C and each alloy was poured 50°C above their specific liquidus temperature. The microstructure of samples was observed by means of an optical microscope Leica DMI 5000 M., equipped with LAS image analyser; the samples were polished up to mirror finishing. Regarding microstructural characterization, Secondary

Dendrite Arm Spacing (SDAS) measurements were performed with the intercept method. Five images at 50x magnification were examined for each alloy and average values and standard deviation were calculated. In addition, grain size was evaluated for the three studied alloys. Samples for grain size measurements were electrochemically etched in a 2% fluoroboric acid (HBF_4) solution and observed under polarised light. Finally, the average area fraction of intermetallic particles for AlSi9CuFe alloy was calculated by means of LAS software for image analysis in order to thoroughly characterize the microstructure of the alloys.

The effect of heat treatment was additionally studied for samples of AlSi9Mg and AlSi9CuFe alloys [14], in order to compare its contribution on material resistance and the influence of intermetallic particles. Samples of both the alloys were solution treated at 520 °C for 4.5 h, then quenched in water at 65°C and aged at 175 °C for 3 h according to industrial parameters for this family of alloys [34].

The average hardness of all the samples (as-cast and heat-treated) was measured by means of Brinell method with a Galileo Ergotest Comp25 apparatus (LTF Galileo Italy) applying a load of 613 N for 10 s and using a ball of 2.5 mm of diameter as an indenter. The measurement was repeated 5 times for each alloy and average values and standard deviation were calculated.

Samples for cavitation tests were machined from the castings as cylinders with diameter of 18 mm and with a proper thread in order to be screwed to the sonotrode, as described in ASTM G32 standard according to the direct method [35]. The test equipment consists of a 20 kHz ultrasonic transducer to which is attached a suitably designed titanium waveguide (Ti6Al4V) and an Inconel 625 horn.

During the experiments, specimen and horn were immersed in a tank filled with tap water, whose temperature was maintained at 25 ± 1 °C. A schematic representation of the testing apparatus is shown in Fig. 1.

Tests were periodically interrupted and samples were removed in order to measure the mass loss as a function of the exposure time, according to the ASTM G32 standard.

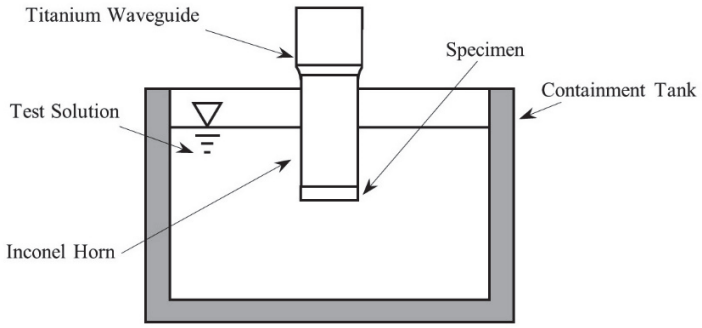

Figure 1: Schematic representation of the experimental set up for cavitation tests.

Three samples were tested for each examined condition in order to obtain reliable results. The total test duration was set at 8 h. Then, the collected data were processed in order to obtain incubation period, erosion rate and total mass loss. The incubation period is defined as the initial stage of the erosion process during which the mass loss is zero or negligible compared to later stages [35].

Furthermore, in order to investigate the evolution of the erosion mechanism, exposed surfaces were observed by means of Scanning Electron Microscope (SEM) LEO EVO 40 coupled with an Oxford Energy Dispersive Spectroscopy (EDS) probe for elemental analysis. In particular, in order to study the initial stages of the erosion process, and to estimate a correlation between cavitation-erosion resistance and alloy microstructure, the samples were observed after 2, 5 and 30 minutes of cavitation exposure. Finally, samples were also analyzed at the end of the test to thoroughly characterize the morphology of the eroded surfaces.

RESULTS AND DISCUSSION

Microstructural characterization

The microstructure of AlSi3 and AlSi9 alloys is shown in Fig. 2. The larger amount of eutectic phase (dark gray in the micrographs) for AlSi9 alloy (Fig. 2b) is due to the higher Si content than in AlSi3 alloy (Fig. 2a), as expected. In fact, according to lever rule, AlSi3 alloy contains approximately 13 wt. % of eutectic phase, while for AlSi9 it raises up to 67 wt. %. After heat treatment, the spheroidization of eutectic Si particles is visible (Fig. 2c).

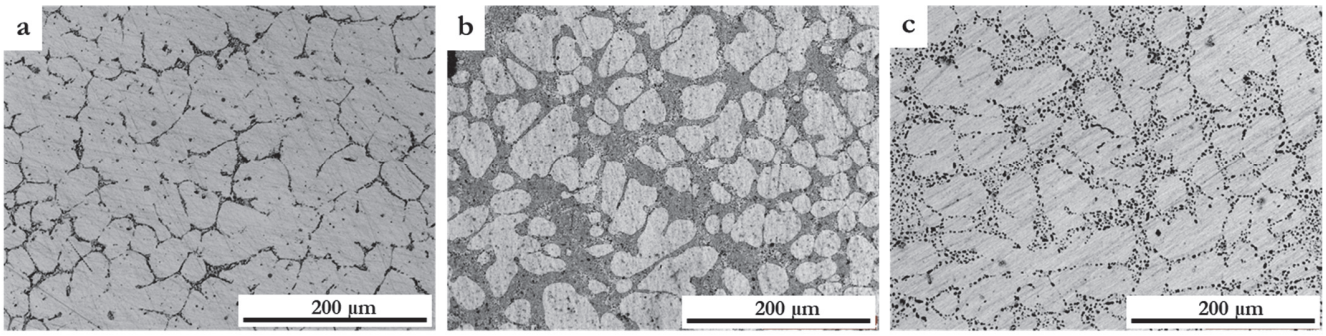

Figure 2: Typical microstructure of a) AlSi3, b) AlSi9, c) AlSi9 T6 alloys.

Analogously to AlSi9 alloy, AlSi9CuFe alloy is characterized by a dendritic microstructure surrounded by eutectic phase in as-cast condition (Fig. 3a), while the heat treatment causes the spheroidization of Si particles (Fig. 3b).

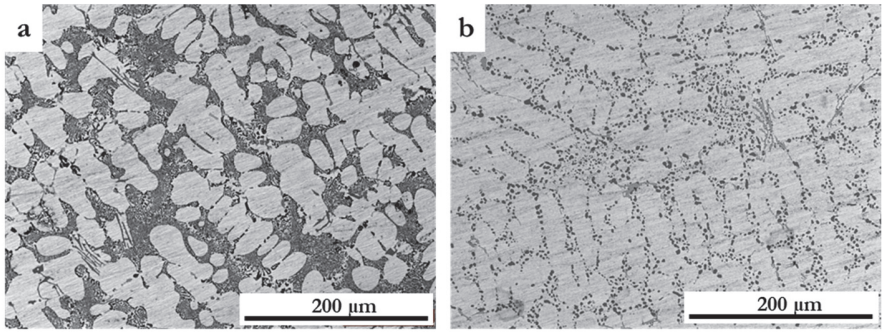

Figure 3: Typical microstructure of a) AlSi9CuFe, b) AlSi9CuFe T6 alloys and c), d) details of intermetallic particles by SEM analysis.

For this alloy, analyses at higher magnification were carried out by means of SEM in order to identify the presence and chemical composition of intermetallic particles, due to the addition of Cu and Fe. As shown in Fig. 4, in fact, several intermetallic compounds with various morphologies (Chinese-script, acicular) were detected. Analyses by EDS probe (Tab. 2) confirmed the presence of significant content of Fe in the composition of most of these coarse particles, while Cu-based intermetallic phases (without Fe) were less abundant and with a finer size. Image analysis allowed identifying an average area fraction of intermetallic phases equal to 2.5 ± 0.2 %. Since intermetallic particles are mainly Fe-based, no significant effect of heat treatment was detected in terms of area fraction [24].

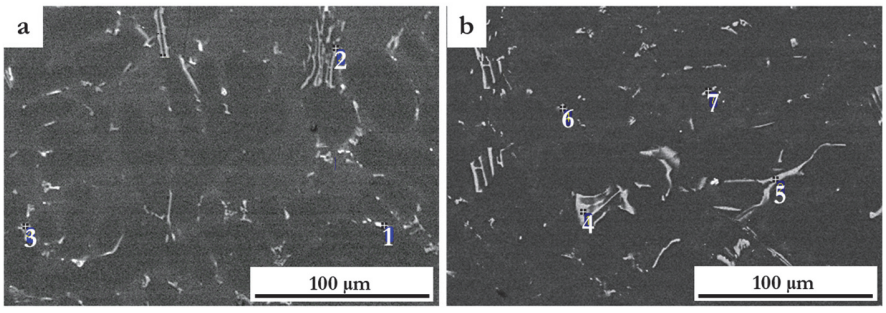

Figure 4: Details of intermetallic particles by SEM analysis for a) AlSi9CuFe, b) AlSi9CuFe T6 alloys.

In order to complete the microstructural characterization of the alloys, calculated values of SDAS and grain size are shown in Tab. 3. It appears that the alloys exhibit comparable values of SDAS, even though slightly lower for AlSi9CuFe, while significant differences were detected in terms of grain size. In fact, AlSi9CuFe alloy is characterized by an average grain size more than double the value measured for the other alloys. This is likely due to the decrease in solidus temperature from 577 °C for AlSi9 alloy to 535 °C for AlSi9CuFe alloy, because of Cu and Fe addition. This means that the solidification

range is significantly wider for the latter alloy and this can lead to a coarsening of grains since pouring and mold temperature were kept constant for all AlSi9 and AlSi9CuFe samples.

	Mg	Al	Si	Cr	Mn	Fe	Ni	Cu
1		63.33	1.14				2.87	32.66
2		61.25	21.33		5.18	12.24		
3	0.62	69.57	8.43	0.55	5.34	11.65	0.60	3.25
4		71.21	7.37		6.20	13.08		2.13
5		59.82	9.78	0.56	8.32	18.62		2.90
6		72.53	8.94	0.78	4.69	10.32	0.91	1.83
7		61.75	14.51	1.26	6.52	12.83	0.90	2.23

Table 2: EDS analysis (wt. %) of the intermetallic particles shown in Fig. 4.

Alloys	SDAS (μm)	Grain size (μm)
AlSi3	31 ± 1	140 ± 6
AlSi9	27 ± 2	160 ± 20
AlSi9CuFe	23 ± 2	350 ± 10

Table 3: Average and standard deviation of SDAS and grain size for the studied alloys.

Finally, Brinell hardness values are reported in Tab. 4. AlSi3 and AlSi9 alloy show comparable hardness, while AlSi9CuFe exhibits a higher value (approximately 20 % higher in comparison with AlSi9 alloy), likely due to the presence of intermetallic particles, which are characterized by greater hardness than the other phases and therefore can positively contribute to enhance this material property [34]. In addition, the effect of the heat treatment leads to an increase in hardness of 56 % for AlSi9 and of 44 % for AlSi9CuFe alloy. This is clearly caused by the precipitation of strengthening particles during T6 heat treatment and demonstrates the effectiveness of the heat treatment parameters applied. In fact, Mg_2Si precipitation takes place in both the alloys since they contain Mg [36]. In addition, Al_2Cu particles precipitates as well in AlSi9CuFe alloy during T6 heat treatment [37].

	AlSi3	AlSi9	AlSi9 T6	AlSi9CuFe	AlSi9CuFe T6
Brinell hardness (HB)	60.2 ± 1.0	62.6 ± 0.5	97.9 ± 0.8	75.8 ± 1.5	109.1 ± 2.4

Table 4: Brinell hardness of the studied alloys.

Cavitation resistance in terms of mass loss

The cavitation resistance of the studied alloys was evaluated in terms of mass loss vs. testing time. In order to make easier the comparison between different materials, first experimental data collected for the alloys tested in as-cast condition are shown in Fig. 5. It appears that the behavior of AlSi3 alloy is significantly different from the other alloys already after the first 30 min of test. The comparison between AlSi3 and AlSi9 alloy is particularly interesting since these alloys exhibit the same hardness and comparable grain size, but a different amount of eutectic. This suggests that the microstructural features that characterize these alloys play an important role in the evolution of erosion mechanism, even though, at the end of the experiments, the total mass loss recorded for AlSi3 and AlSi9 alloy is fairly similar (Tab. 5).

On the other hand, AlSi9 and AlSi9CuFe alloys lost approximately the same mass during the first 5 h of testing, while for longer exposure a significant difference in material behavior emerges, with AlSi9CuFe exhibiting the greatest resistance to cavitation erosion. In detail, it showed a total mass loss about 18% lower than the corresponding alloy without intermetallics

and about 24% lower than the AlSi3. In this case, the main microstructural differences between the AlSi9 and AlSi9CuFe alloys are the presence of intermetallic particles and grain size.
Concerning the maximum erosion rate of the three compositions, the increase of eutectic percentage, from AlSi3 to AlSi9, determines a reduction of about 27%, while the presence of Cu and Fe intermetallic does not considerably affect this parameter.
As aforementioned, grain size is reported to have a significant influence on mechanical properties. In particular, regarding cavitation erosion, it is reported that fine grain structure leads to an increase in surface density of grain boundaries, which provide a positive supporting action in hindering the movement of dislocation and, therefore, preventing material removal [38]. The presence of coarse grains for AlSi9CuFe alloy reduces the surface density of grain boundaries and this is expected to reduce the material resistance. On the other hand, the presence of intermetallic particles with complex morphology is supposed to be beneficial since they cannot be easily dislodged from the metal matrix, reinforcing the primary phase and thus enhancing the alloy performances [20]. Hence, this suggests that intermetallic particles play a dominant role in comparison with that of grain size in defining cavitation erosion resistance. However, to confirm this assumption, the observation of eroded surfaces is a necessary step to provide a proper interpretation of the erosion mechanism.

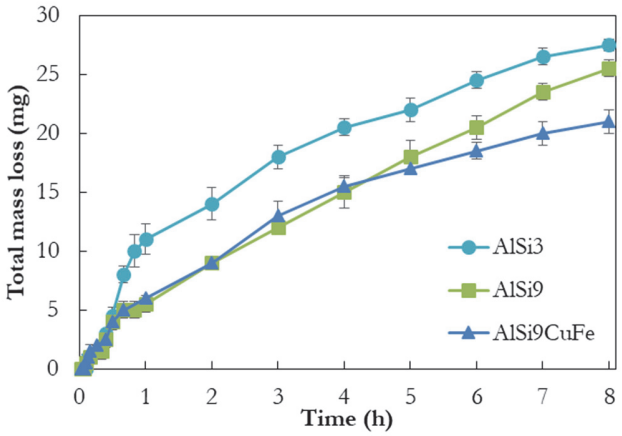

Figure 5: Mass loss values during cavitation tests for the alloys in as-cast condition.

The effect of T6 heat treatment is presented in Fig. 6, where the results for each alloy in as-cast condition are compared with the corresponding performance after heat treatment. As expected [14, 19-20], the heat treatment provides a beneficial effect on cavitation resistance since the mass loss diminishes of approximately 25 % for AlSi9 and of 17 % for AlSi9CuFe alloy. Particularly, the incubation period (Tab. 5) is clearly affected by the heat treatment. In fact, the uniform distribution of fine precipitates in the Al matrix hinders material removal resulting in a longer duration of the incubation stage for the alloys in T6 condition. Finally, it can be clearly noticed how the T6 treatment affects the maximum erosion rate, inducing a reduction of about 25% and 44% for the AlSi9 and AlSi9CuFe respectively.

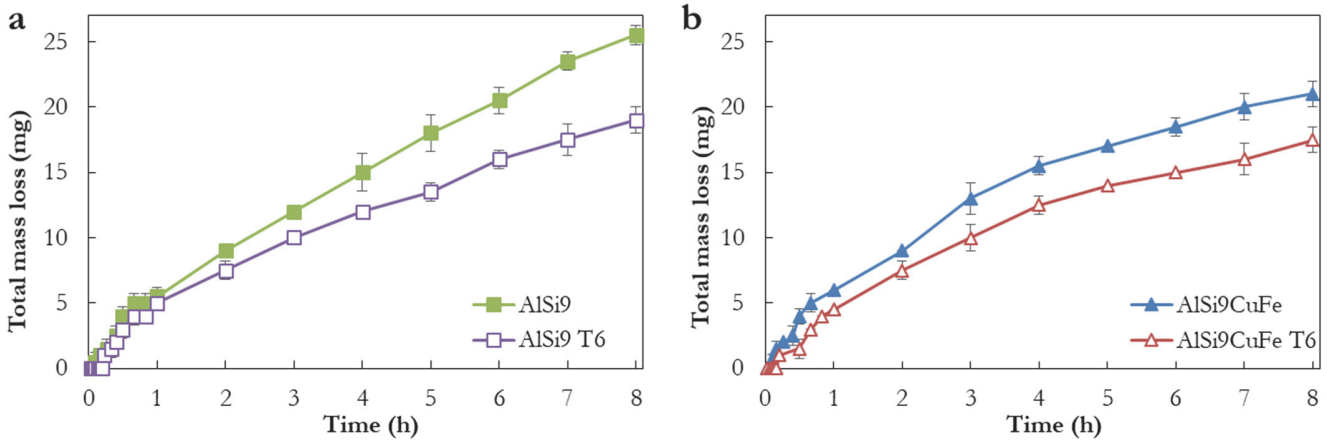

Figure 6: Effect of heat treatment on cavitation erosion resistance for a) AlSi9 and b) AlSi9CuFe alloy.

Alloys	Incubation period (min)	Total mass loss (mg)	Maximum erosion rate (mg/h)
AlSi3	8	27.5 ± 0.5	11
AlSi9	7	25.5 ± 0.7	8
AlSi9 T6	14	19.0 ± 1.0	6
AlSi9CuFe	8	21.0 ± 1.0	8
AlSi9CuFe T6	12	17.5 ± 1.0	4.5

Table 5: Incubation period, total mass loss and maximum erosion rate for the studied alloys.

The evolution of the erosion rate during the test is illustrated in Fig. 7 as a function of testing time. According to ASTM G32 [35], it is possible to identify the five main stages of erosion, which are indicated as incubation, acceleration, maximum rate, deceleration and terminal stage. It is interesting to note that the first three phases take place in the first hour of testing for all the studied alloys, with a steep increase of erosion rate, which subsequently diminishes until it reaches quite constant values during the second half of the test. This indicates a tendency towards a linear erosion mechanism with a constant erosion rate, in the range of 1-3 mg/h, regardless the chemical composition and the hardness for the investigated Al-Si alloys.

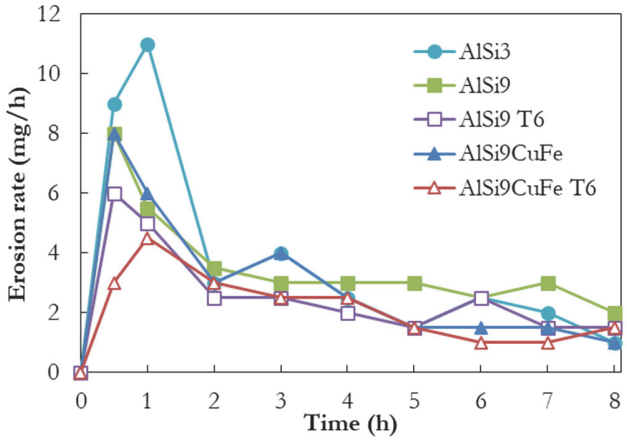

Figure 7: Evolution of erosion rate during cavitation tests for the studied alloys.

Since several authors proposed a correlation between mass loss and material hardness for alloys belonging to the same family, the corresponding values for the studied alloys were plotted, as shown in Fig. 8. A fairly linear relationship between the two parameters can be observed, even though R^2 value is not optimal (0.95), confirming the general observation that a clear correlation cannot be stated [14-15].
In order to thoroughly study the cavitation erosion mechanism, SEM analysis of eroded surfaces was carried out after various exposure duration. This it is necessary to identify the influence of microstructural parameters and provide a complete interpretation of the erosion mechanism.

Investigation of eroded surfaces: effect of Si content.
First, the effect of different Si content was investigated through the observation of the eroded surfaces of AlSi3, AlSi9 and AlSi9 T6 samples after short time exposures.
Particularly, representative images after 2 minutes of testing are shown in Fig. 9. It can be appreciated that AlSi3 alloy (Fig. 9a) exhibits the most deformed surface, with secondary phases emerging slightly from the surface due to the plastic deformation of the Al matrix, as confirmed by EDS analysis (Tab. 6). A similar behavior can be noticed for AlSi9 alloy (Fig. 9b), where the abundant eutectic phase does not exhibit evident modification, while the Al matrix is affected by undulation due to plastic deformation. This is a confirmation that the Al matrix in the primary site for erosion, as reported in previous studies by the authors [9, 10].

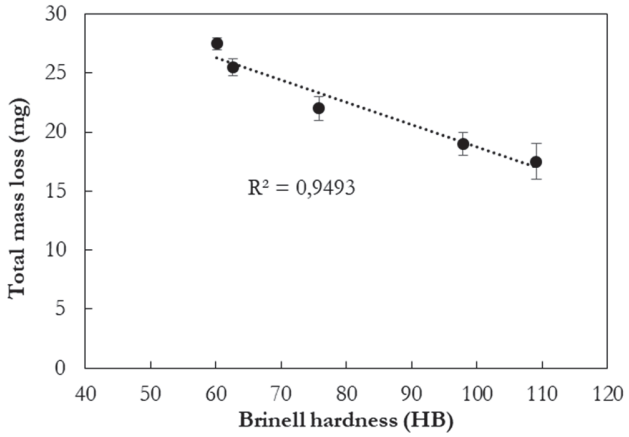

Figure 8: Correlation between mass loss and material hardness.

As aforementioned, the strengthening of the Al matrix after heat treatment improves its cavitation erosion resistance [14, 19-20] and, consequently, a low degree of plastic deformation is present on the surface of AlSi9 T6 sample (Fig. 9c) where, at this stage, it is not possible to distinguish between different phases.

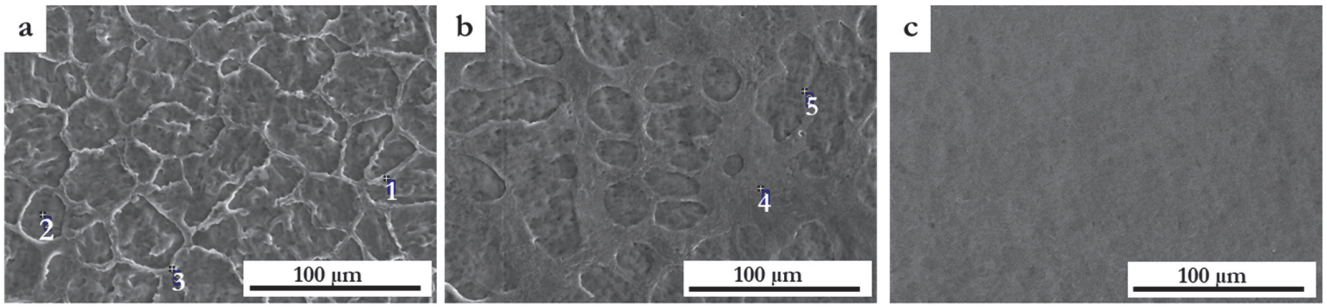

Figure 9: Eroded surfaces after 2 minutes of cavitation test for a) AlSi3, b) AlSi9, c) AlSi9 T6 alloys.

	Mg	Al	Si
1	1.44	96.63	1.93
2		95.52	4.48
3	0.81	85.68	13.51
4		80.59	19.41
5		98.14	1.86

Table 6: EDS analysis (wt. %) for SEM images in Fig. 9.

After 5 min of testing, the morphology of eroded surfaces of AlSi3 and AlSi9 alloys (Fig. 10a-b) are similar and a corrugation of the eutectic phase is now visible for AlSi9 alloy. On the other hand, after 5 min, the heat-treated sample (Fig. 10c) shows only a slight undulation of the surface. Nevertheless, in comparison with the previous analysis performed after shorter exposure time, some pits appeared due to the repetition of micro-jets. The slower erosion of AlSi9 T6 sample is consistent also with the higher incubation period, recorded from mass loss measurements (Tab. 5).
The influence of microstructure can be no longer observed after 30 min of cavitation exposure (Fig. 11). In fact, at this stage, the erosion mechanism was already at an advanced stage and all the investigated alloys exhibited a certain mass loss (Fig. 5-6). The corrugation of the eroded surfaces appears uniform and with a morphology that resembles that of ductile fracture [19].

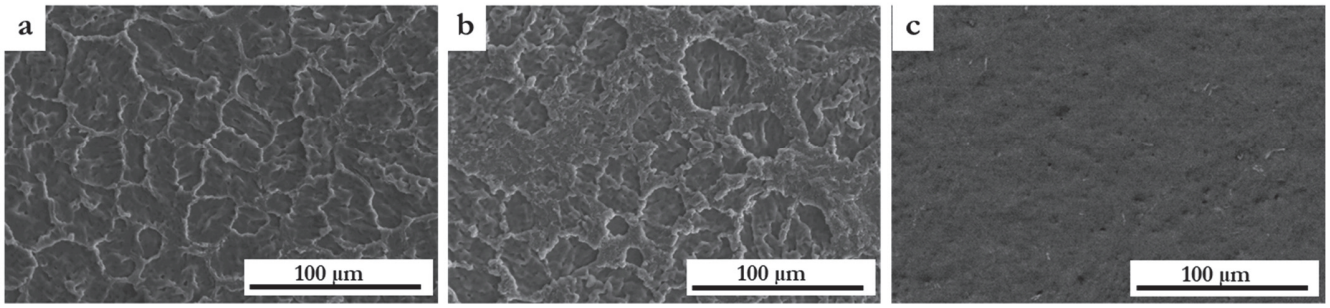

Figure 10: Eroded surfaces after 5 minutes of cavitation test for a) AlSi3, b) AlSi9, c) AlSi9 T6 alloys.

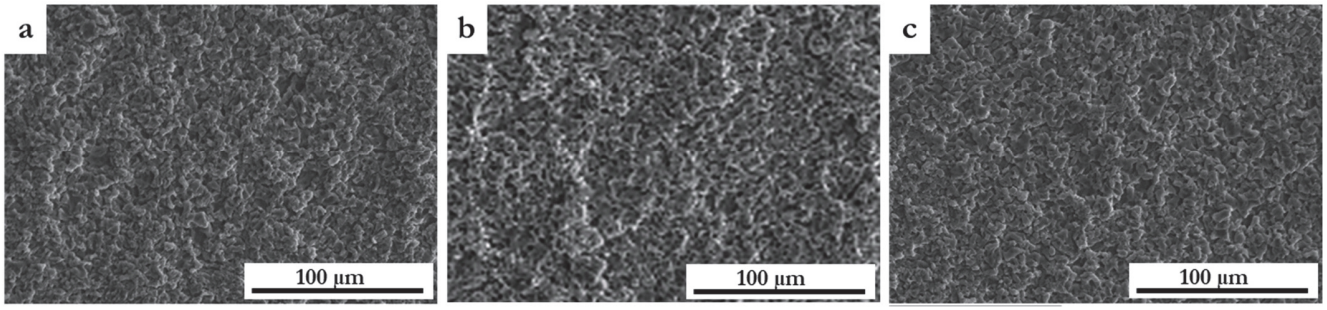

Figure 11: Eroded surfaces after 30 minutes of cavitation test for a) AlSi3, b) AlSi9, c) AlSi9 T6 alloys.

Images at lower magnification are provided in Fig. 12 in order to appreciate the degree of damage after 8 h of testing. Large craters are visible for all the alloys. AlSi3 alloy exhibited the largest craters, while AlSi9 T6 sample was less damaged. The craters likely originated in correspondence of casting defects and then grew with consequent material removal due to fracture of the rim of the craters or flaking [1].

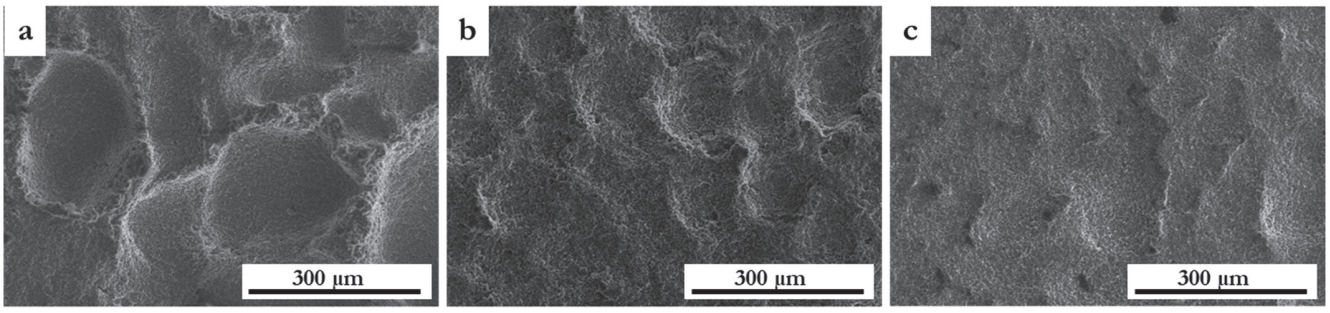

Figure 12: Eroded surfaces after 8 h of cavitation test for a) AlSi3, b) AlSi9, c) AlSi9 T6 alloys.

To summarize, at initial stages of erosion, the Al matrix is more prone to deformation, and subsequently erosion, in comparison with the eutectic phase, which is less affected by the load condition due to cavitation. This is especially evident for AlSi3 alloy since it is characterized by the highest area fraction of Al matrix. This is responsible for a larger material removal for AlSi3 alloy in comparison with AlSi9 alloy, despite their similar hardness and grain size. On the other hand, when the Al matrix is strengthened by the formation of precipitates due to heat treatment, the erosion process is delayed, resulting in an increase in incubation period and a decrease in total mass loss and maximum erosion rate.

Investigation of eroded surfaces: Effect of intermetallic particles.

Analogously, the eroded surfaces of AlSi9CuFe alloy in as-cast and heat-treated condition were evaluated in order to investigate the role of intermetallic particles. Since these compounds are characterized by the presence of elements with high atomic weight, images acquired in back-scattered mode are shown for easier detection of intermetallic particles.

After 2 min of cavitation test, besides the aforementioned different degree of plastic deformation of the Al matrix due to the heat treatment, intermetallic particles are clearly visible on the surface of both samples and appear unaffected by the erosion mechanism (Fig. 13).

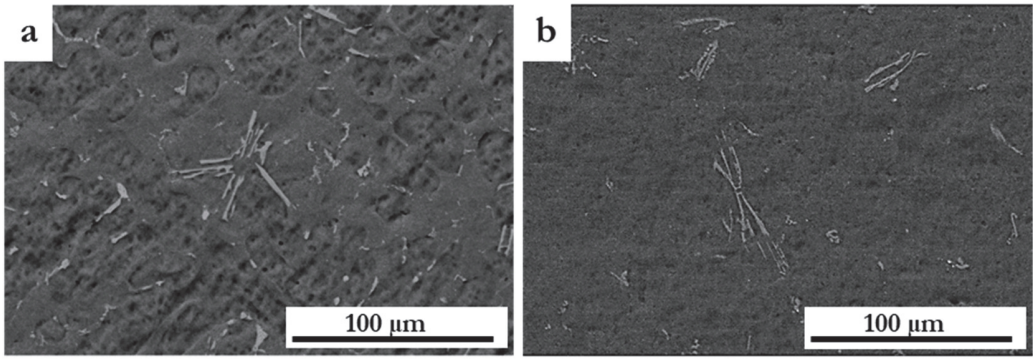

Figure 13: Eroded surfaces after 2 minutes of cavitation test for a) AlSi9CuFe, b) AlSi9CuFe T6 alloys.

In order to better appreciate their influence, the same area was observed for AlSi9CuFe samples after 2 and 5 minutes of cavitation exposure (Fig. 14). In particular, it was chosen an area where a crater was already present, likely due to a pre-existent porosity. It can be seen that intermetallic particles located on the edge of the crater (white circles) are not removed by prolonged cavitation exposure, while material removal took place on the other sides of the crater itself, as indicated by arrows. As found also for other Al-Si alloys in a previous study [20], intermetallic particles, especially with a complex morphology, can provide additional cavitation resistance, preventing material removal.

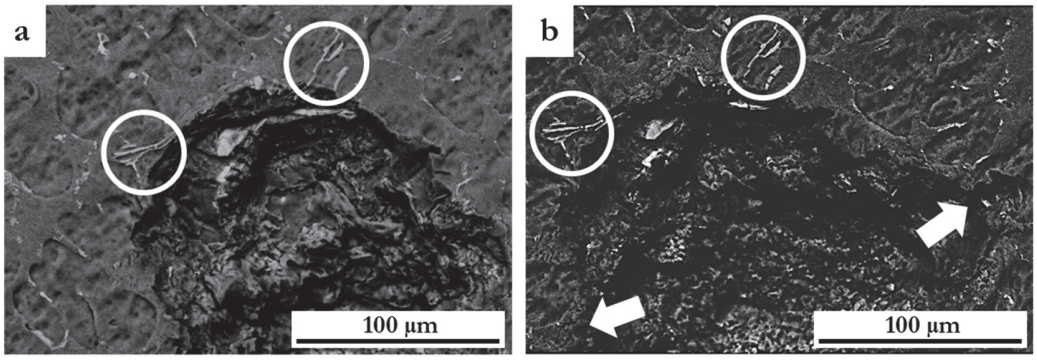

Figure 14: SEM images of the same area on the eroded surface of AlSi9CuFe samples after a) 2 min and b) 5 min of cavitation testing.

As discussed for the other alloys, after 30 min of testing, a uniform material removal took place and it is not possible to identify a different deformation for diverse phases anymore (Fig. 15).

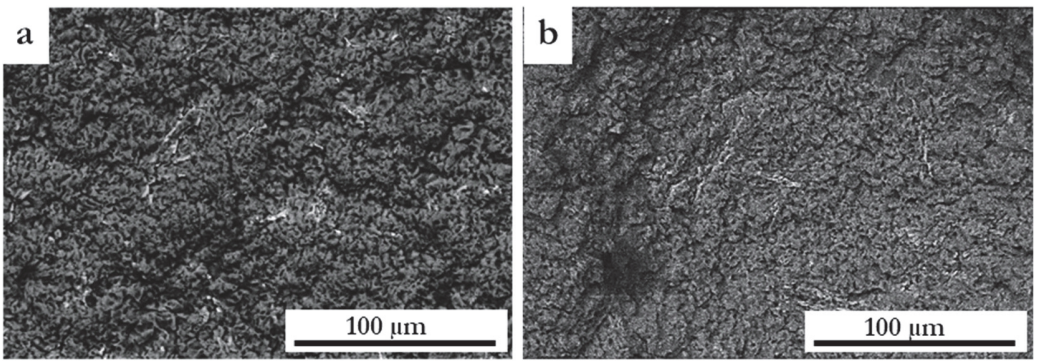

Figure 15: Eroded surfaces after 30 minutes of cavitation test for a) AlSi9CuFe, b) AlSi9CuFe T6 alloys.

Some intermetallic particles are visible on the damaged surface both in as-cast and heat-treated condition after 30 min of exposure, as well as after 8 h (Fig. 16). They likely belong to underlying areas of the alloy and are exposed after progressive material removal. In general, it is believed that their abundant presence hinders plastic deformation and material removal, at advanced stage of cavitation erosion, in agreement with the mass loss curves shown in Fig. 5.
Nevertheless, for AlSi9CuFe alloy, this contribution is not significantly affecting the incubation period, which is comparable to the values measured for AlSi3 and AlSi9 alloy, contrary to what found in a previous study by the authors [20]. This is likely due to the elongated morphology of the particles in AlSi9CuFe alloy. In fact, according to the experimental evidences [20], coarse and polygonal intermetallic particles were responsible for longer incubation period, besides lower mass loss, in comparison with acicular compounds. In the present case, instead, intermetallic particles are very numerous, but their elongated shape can be responsible for stress concentration [39] and for their easier removal during erosion test in comparison with more rounded particles [40]. Furthermore, it is reported [41] that the direct method used in the present study accelerate the erosion mechanism in comparison with the indirect method used in the previous one. Therefore, this can lead to a general decrease in the incubation period and can make more difficult to identify differences between different alloys.

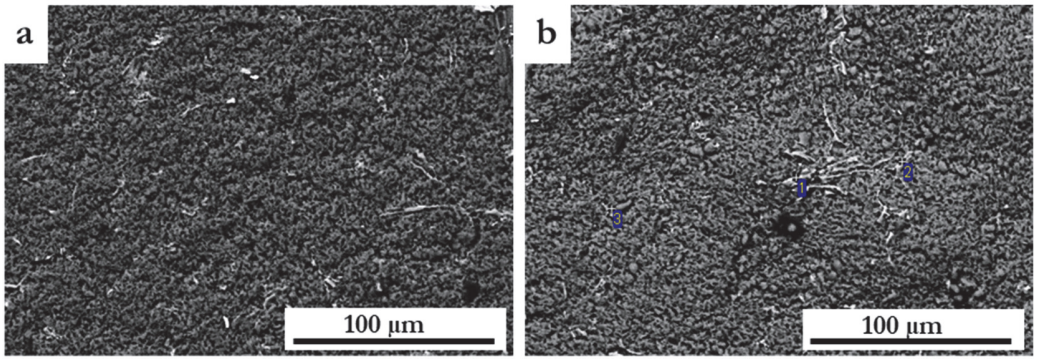

Figure 16: Eroded surfaces after 8 h of cavitation test for a) AlSi9CuFe, b) AlSi9CuFe T6 alloys.

Conclusions

The cavitation erosion resistance of three Al-Si alloys was studied in order to individuate the influence of microstructural parameters and material hardness. It was found that the increase in Si content, and therefore a larger eutectic phase, is beneficial to the alloy performance since this phase is less affected than the Al matrix by the cyclic load associated with bubbles collapse due to cavitation phenomenon. This especially leads to a decrease in total mass loss and maximum erosion rate. In addition, the strengthening of the Al matrix because of heat treatment delays material removal resulting in an increase in the incubation period, with consequent positive effect on the overall material performance. Finally, according to the findings, it is believed that intermetallic particles with complex morphology can provide an additional contribution to improve cavitation erosion resistance of the studied alloys, as demonstrated by the lowest total mass loss measured forAlSi9CuFe alloy. A general trend of decreasing total mass loss with increasing hardness was found, even if a linear correlation between these two parameters cannot be stated.

References

[1] Davis, J. R., Corrosion of Aluminum and Aluminum Alloys, ASM International, (1999).
[2] Okada, T., Iwai, Y., Hattori, S., Tanimura, N., Relation between impact load and the damage produced by cavitation bubble collapse, Wear, 184 (1995) 231-239.
[3] Vyas, B., Preece, C. M., Cavitation Erosion of Face Centered Cubic Metals, Metall. Trans. A, 8A (1977) 915-923.
[4] Hansson, I., Morch, K. A., The initial stage of cavitation erosion on aluminium in water flow, J. Phys. D: Appl. Phys., 11 (1978) 147-154.
[5] Preece, C. M., Macmillan, N. H., Erosion, Ann. Rev. Mater. Sci., 7 (1977) 95-121.

[6] Kwok, C. T., Cheng, F. T., Man, H. C., Synergistic effect of cavitation erosion and corrosion of various engineering alloys in 3.5% NaCl solution, Mater. Sci. Eng. A, 290 (2000) 145-154.
[7] dos Santos, J. F., Garzón, C. M., Tschiptschin, A. P. Improvement of the cavitation erosion resistance of an AISI 304L austenitic stainless steel by high temperature gas nitriding, Mater. Sci. Eng. A, 382 (2004) 378-386.
[8] Hattori, S., Kitagawa, T., Analysis of cavitation erosion resistance of cast iron andnonferrous metals based on database and comparison with carbon steel data, Wear, 269 (2010) 443-448.
[9] Neville, A., McDougall, B. A. B., Erosion– and cavitation–corrosion of titanium and its alloys, Wear, 250 (2001) 726-735.
[10] Li, H., Cui, Z., Li, Z., Zhu, S., Yang, X., Effect of gas nitriding treatment on cavitation erosion behavior of commercially pure Ti and Ti-6Al-4V alloy, Surf. Coat. Technol., 221 (2013) 29-36.
[11] Richman, R. H., McNaughton, W. P., Correlation of cavitation erosion behavior with mechanical properties of metals, Wear, 140 (1990) 63-82.
[12] Fortes Patella, R., Choffat, T., Reboud, J.-L., Archer, A., Mass loss simulation in cavitation erosion: Fatigue criterion approach, Wear, 300 (2013) 205-215.
[13] Sreedhar, B. K., Albert, S. K., Pandit, A. B., Cavitation damage: Theory and measurements - A review, Wear, 372-373 (2017) 177-196.
[14] Vaidya, S., Preece, C. M., Cavitation Erosion of Age-Hardenable Aluminum Alloys, Metall. Trans. A, 9A (1978) 299-307.
[15] Pola, A., Montesano, L., Tocci, M., La Vecchia, G. M., Influence of Ultrasound Treatment on Cavitation Erosion Resistance of AlSi7 Alloy, Materials, 10 (2017) 256.
[16] Ye, H., An Overview of the Development of Al-Si-Alloy Based Material for Engine Applications, J. Mater. Eng. Perform., 12 (2003) 288-297.
[17] Lee, S. J., Kim, K. H., Kim, S. J., Surface Analysis of Al-Mg Alloy Series for Ship after Cavitation Test, Surf. Interface Anal., 44 (2011) 1389-1392.
[18] Laguna-Camacho, J. R., Lewis, R., Vite-Torres, M., Méndez-Méndez, J. V., A study of cavitation erosion on engineering materials, Wear, 301 (2013) 467-476.
[19] Tomlinson, W. J., Matthews, S. J., Cavitation erosion of aluminium alloys, J. Mater. Sci., 29 (1994) 1101-1108.
[20] Gottardi, G., Tocci, M., Montesano, M., Pola, A., Cavitation erosion behaviour of an innovative aluminium alloy for Hybrid Aluminium Forging, Wear, 394-395 (2018) 1-10.
[21] Dwivedi, D. K., Sharma, R., Kumar, A., Influence of silicon content and heat treatment parameters on mechanical properties of cast Al–Si–Mg alloys, Int. J. Cast Metal. Res., 19 (2006) 275-282.
[22] Wang, Y., Liao, H., Wu, Y., Yang, J., Effect of Si content on microstructure and mechanical properties of Al–Si–Mg alloys, Mater. Des., 53 (2014) 634-638.
[23] Ceschini, L., Boromei, I., Morri, A., Seifeddine, S., Svensson, I. L., Effect of Fe content and microstructural features on the tensile and fatigue properties of the Al-Si10-Cu2 alloy, Mater. Des., 36 (2012) 522-528.
[24] Taylor, J. A., Iron-containing intermetallic phases in Al-Si based casting alloys, Proc. Mat. Sci., 1 (2012) 19-33.
[25] Tocci, M., Donnini, R., Angella, G., Pola, A., Effect of Cr and Mn addition and heat treatment on AlSi3Mg casting alloy, Mater. Charact., 123 (2017) 75-82.
[26] Basavakumar, K. G., Mukunda, P. G., Chakraborty, M., Influence of grain refinement and modification on microstructure and mechanical properties of Al-7Si and Al-7Si-2.5Cu cast alloys, Mater. Charact., 59 (2008) 283-289.
[27] Casari, D., Merlin, M., Garagnani, G. L., A comparative study on the effects of three commercial Ti-B-based grain refiners on the impact properties of A356 cast aluminium alloy, J. Mater. Sci., 48 (2013) 4365-4377.
[28] Zhao, W., Zhang, L., Wang, Z., Yan, H., Study on Defects of A356 Aluminum Alloy Wheel, Adv. Mat. Res., 189-193 (2011) 3862-3865.
[29] Tomlinson, W. J., Matthews, S. J., Cavitation erosion of aluminium alloy matrix/ceramic composites, J. Mater. Sci. Lett., 13 (1994) 170-173.
[30] Ćosić, M., Dojčinović, M., Aćimović-Pavlović, Z., Fabrication and behaviour of Al-Si/SiC composite in cavitation conditions, Int. J. Cast. Metal. Res., 27 (2014) 49–55.
[31] Sjolander, E., Seifeddine, S., Optimisation of solution treatment of cast Al–Si–Cu alloys, Mater. Des., 31 (2010) 44-49.
[32] Han, Y., Samuel, A. M., Doty, H. W., Valtierra, S., Samuel, F. H., Optimizing the tensile properties of Al–Si–Cu–Mg 319-type alloys: Role of solution heat treatment, Mater. Des., 58 (2014) 426-438.
[33] Tocci, M., Pola, A., Raza, L., Armellin, L., Afeltra, U., Optimization of heat treatment parameters for a nonconventional Al-Si-Mg alloy with cr addition by DoE method, Metall. Ital., 108 (2016) 141-144.

[34] Davis, J. R., ASM Speciality Handbook, Aluminum and Aluminum Alloys, ASM International, Davis & Associates, Materials Park, OH, 1993.
[35] ASTM. ASTM G32. Standard test method for cavitation erosion using vibratory apparatus.
[36] Wang, Q. G., Davidson, C. J., Solidification and precipitation behaviour of Al-Si-Mg casting alloys, J. Mat. Sci., 26 (2001) 739-750.
[37] Reif, W., Dutkiewicz, J., Chiach, R., Yu, S., Krol, J., Effect of ageing on the evolution of precipitates in AlSiCuMg alloys, Mater. Sci. Eng. A, 234-236 (1997) 165-168.
[38] Bregliozzi, G., Di Schino, A., Ahmed, S. I.-U., Kenny, J. M., Haefke, H., Cavitation wear behaviour of austenitic stainless steels with different grain sizes, Wear, 285 (2005) 503-510.
[39] Moustafa, M. A., Samuel, F. H., Doty, H. W., Effect of solution heat treatment and additives on the microstructure of Al–Si (A413.1) automotive alloys, J. Mater. Sci., 38 (2003) 4507-4522.
[40] Hovis, S. K., Talia, J., Scattergood, R. O., Erosion mechanisms in aluminum and Al-Si alloys, Wear, 107 (1986) 175-181.
[41] Cojocaru, V., Campian, V. C., Frunzaverde, D., A comparative analysis of the methods used for testing the cavitation erosion resistance on the vibratory devices, U.P.B. Sci. Bull., Series D, 77 (2015) 257-262.